RESEARCH ARTICLE

Analytical Kinematic Modeling and Simulation Verification of a Three-Link Planar Manipulator

Nuoyu Jiang[1,*]

[1] School of Electrical Engineering, Yancheng Institute of Technology, Yancheng 224051, China

Abstract

This paper establishes an analytical kinematic model for a three-degree-of-freedom planar manipulator with three serial links, and validates it through MATLAB numerical simulations and SolidWorks-ADAMS co-simulation. Based on the mechanism topology and the Denavit-Hartenberg (D-H) parameter method, coordinate frames are assigned, and homogeneous transformation modeling is performed, leading to a closed-form forward kinematics expression for the end-effector pose. By combining wrist-point decomposition, geometric approaches, and the law of cosines, an analytical inverse kinematics solution is derived, and the characteristics of multiple solution configurations are discussed. The simulation results show that the analytical forward and inverse kinematics are consistent with the numerical outputs from the Robotics Toolbox, and the inverse solution can reliably recover the joint angles. In the ADAMS simulation, joint responses follow a sinusoidal driving law, and the end-effector trajectory is continuous and smooth, satisfying the motion characteristics of planar mechanisms. These results confirm the correctness and engineering applicability of the proposed model.

Keywords: three-link planar manipulator, D-H parameter method, forward kinematics, analytical inverse kinematics, MATLAB and ADAMS simulation validation.

1 Introduction

With the continuous advancement of industrial robots and their control technologies, robotic automation has become one of the key approaches for modern manufacturing to enhance productivity, ensure product consistency, and realize flexible production [1]. Industrial robots can replace or assist human labor in tasks that are highly repetitive, hazardous, or require stringent stability and precision, and they have been widely applied in automotive manufacturing, 3C electronics assembly, metal processing, food packaging, pharmaceutical sorting, and warehouse logistics [2–6]. According to ISO 8373:2012, an industrial robot is defined as "an automatically controlled, reprogrammable, multipurpose manipulator, programmable in three or more axes, used in industrial automation applications" [7]. This definition highlights the essential features of multi-axis programmability and task transferability, providing a unified conceptual framework for manipulator structural design and control research. The stable operation of industrial robots in practical production relies on the coordinated performance of actuator driving, sensor feedback, and control algorithms [8]. In this process, the controller

Submitted: 06 January 2026
Accepted: 03 February 2026
Published: 13 February 2026

Vol. 1, **No.** 1, 2026.
10.62762/TICPS.2026.746937

***Corresponding author:**
✉ Nuoyu Jiang
jiangnuoyu2025@126.com

Citation
Jiang, N. (2026). Analytical Kinematic Modeling and Simulation Verification of a Three-Link Planar Manipulator. *ICCK Transactions on Intelligent Cyber-Physical Systems*, 1(1), 26–37.

precisely schedules joint variables to enable the end-effector to achieve the desired pose and trajectory in task space [9].

From the perspective of technological evolution and industrial demand, industrial robots are being upgraded from traditional "preprogrammed automation" toward "intelligent collaboration in complex environments" [10]. With the advancement of intelligent manufacturing and Industry 4.0/5.0, robotic systems are required to maintain stable operational capability in high-mix low-volume production, rapid line changeovers, and uncertain environments [11–13]. However, existing robots still exhibit limitations in task transfer, environmental adaptability, and autonomous planning [14–16]. In particular, under complex constraints or external disturbances, motion planning and control performance depend heavily on the accuracy and interpretability of the manipulator's kinematic model [17]. Although intelligent perception and decision-making technologies have been developing rapidly [18–23], fundamental kinematic modeling remains a prerequisite for trajectory generation, error compensation, and control-law design. Its rigor is directly related to the engineering applicability and operational safety of robotic systems [24, 25].

Among various industrial robot configurations, serial articulated manipulators are the most common due to their versatile structure, large workspace, and flexible posture adjustment capability [26]. Although industrial applications often employ spatial manipulators with six or more degrees of freedom to meet complex task requirements, low-DOF manipulators remain representative in education and research, lightweight operations, and specific automation cells, owing to their simple structure, clear control logic, and low cost [27]. Kinematic studies on serial manipulators aim to establish the mapping between joint space and task space: forward kinematics determines the end-effector pose for a given set of joint variables, whereas inverse kinematics computes the corresponding joint angles for a specified end-effector target pose [28]. Due to the geometric characteristics of serial mechanisms, inverse kinematics is often associated with multiple solutions, singular configurations, and reachable-boundary issues [29]. These properties not only determine the feasibility of trajectory planning but also directly affect the stability and safety of robot operation.

Against this background, this paper investigates a three-link planar manipulator, focusing on its kinematic modeling, analytical solutions, and simulation-based consistency verification. The three-link planar manipulator is a typical fundamental unit of serial manipulators. With relatively low model complexity, it fully reflects key problems such as D-H parameter-based modeling, analytical forward and inverse kinematics, multi-solution configuration analysis, and singularity discussion. Therefore, it has strong theoretical representativeness and methodological demonstrative value. To ensure the engineering reliability of the analytical model, this study further performs closed-loop validation by combining numerical simulations with three-dimensional dynamic simulations. Specifically, cross-verification and error comparison of forward and inverse solutions are conducted in the MATLAB Robotics Toolbox, while a physical multibody model is established in the SolidWorks-ADAMS platform. Under periodic driving inputs, joint responses and end-effector trajectory characteristics are analyzed to examine the consistency between the analytical derivations and the actual motion behavior.

The remainder of this paper is organized as follows. Section 2 introduces the basic concepts of robot kinematics and the D-H parameter modeling method. Section 3 derives the analytical forward and inverse kinematic models of the 3-DOF three-link planar manipulator and discusses its multiple-solution characteristics. Section 4 presents numerical and three-dimensional simulation validation of the analytical model using MATLAB and ADAMS.

2 Fundamentals of Robot Kinematics

This chapter reviews the basic concepts and modeling methods of robot kinematics, providing the theoretical foundation for the derivation and simulation of the forward and inverse kinematics of a three-link planar manipulator. Using the Denavit-Hartenberg (D-H) parameter method [30], serial manipulators are modeled in a standardized manner. The criteria for establishing link coordinate frames and the homogeneous transformation matrix between adjacent links are presented, thereby offering a unified description of the mapping from joint space to task space.

2.1 Overview of Robot Kinematics

Robot kinematics is a fundamental theory for analyzing the relationship between robot structure and motion. Its core objective is to establish a mapping

between joint-space variables and task-space poses. For manipulator systems, kinematic analysis does not involve dynamic factors such as forces and torques; instead, it focuses on how variations in joint variables lead to changes in the position and orientation of the end-effector.

In general, robot kinematics mainly includes the following aspects:

- *Forward kinematics*: given the joint variables, the spatial position and orientation of the end-effector in the base coordinate frame are determined. Forward kinematics provides an explicit geometric description for trajectory generation, workspace analysis, and simulation.
- *Inverse kinematics*: for a specified target pose of the end-effector, the corresponding joint variables are solved in reverse. Inverse kinematics is a core problem in robot path planning, posture control, and online motion computation, and it typically involves multiple solutions and configuration selection.
- *Velocity/acceleration kinematics*: by constructing the Jacobian matrix, the mapping between joint velocities and the end-effector's linear and angular velocities is described, providing the mathematical basis for dynamic modeling, controller design, and real-time motion planning. Therefore, establishing a unified, standardized, and generalizable kinematic modeling method is a prerequisite for accurate motion analysis and control of robots.

2.2 Kinematic Analysis of Robots

Robot kinematic analysis aims to describe the geometric motion laws exhibited by a manipulator as its position and orientation change in space, without considering the driving forces required to generate such motion. To systematically and in a standardized manner represent the link-joint relationships of serial manipulators, the D-H parameter method is widely adopted for robot modeling. The D-H approach assigns a local coordinate frame to each link and uses four geometric parameters to characterize the relative position and orientation between two adjacent link frames. In this way, the spatial motion of a complex mechanism can be decomposed into a sequence of simple and computable coordinate transformations.

2.2.1 Manipulator Links and D-H Parameters

A manipulator can be regarded as a kinematic chain formed by multiple rigid bodies connected in series through joints, where each rigid body is referred to as a link. In engineering design, links must be determined by considering factors such as material properties, stiffness, mass, and dimensions. In kinematic modeling, however, links are usually idealized as rigid bodies to simplify the analysis, and only the geometric relationship between each link and its adjacent joint axes is considered.

In three-dimensional space, the relative configuration between two adjacent links can be uniquely described by four D-H parameters, as illustrated in Figure 1.

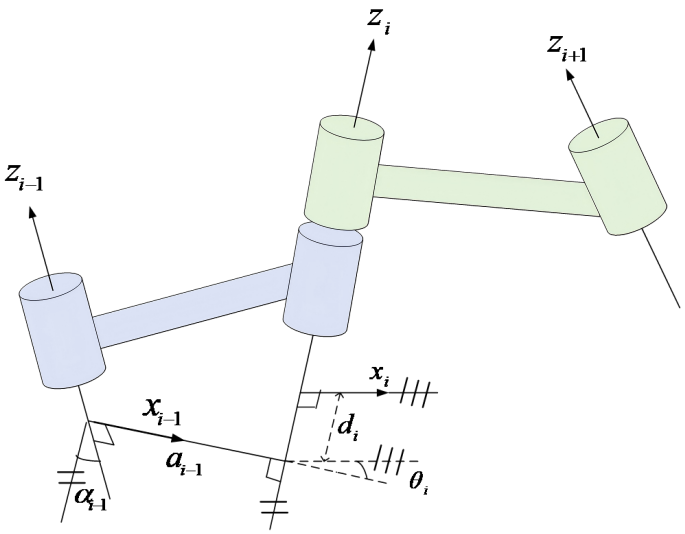

Figure 1. Relationship between manipulator links.

The parameters in Figure 1 are defined as follows:

- Link length a_{i-1}: the length of the common normal between the joint axes z_{i-1} and z_i.
- Link twist angle α_{i-1}: the angle from z_{i-1} to z_i measured by a rotation about the x_{i-1} axis.
- Link offset d_i: the distance along the z_{i-1} axis from x_{i-1} to x_i.
- Joint angle θ_i: the angle from x_{i-1} to x_i measured by a rotation about the z_i axis.

For a manipulator, joints are typically classified into two types: prismatic joints and revolute joints. In a prismatic joint, d_i is the joint variable, while a_{i-1}, α_{i-1}, and θ_i are constants. In a revolute joint, θ_i is the joint variable and the remaining parameters are constants. Therefore, the four D-H parameters provide a standardized representation of the geometric

relationships in complex serial manipulators, forming a unified framework for subsequent homogeneous transformations and kinematic solutions.

2.3 Establishment of Link Coordinate Frames

To describe the relative pose between adjacent links, a right-handed coordinate frame $\{i\}$ is attached to each link. The base frame $\{0\}$ is fixed to the robot base and is also referred to as the world frame, while $\{i\}$ denotes the frame attached to the i-th link. The z_i-axis of frame $\{i\}$ usually coincides with the axis of joint $i+1$. For a revolute joint, the positive direction of z_i follows the right-hand rule, whereas for a prismatic joint, z_i is aligned with the direction of translation.

When the joint axes z_{i-1} and z_i intersect, their intersection point is chosen as the origin of frame $\{i\}$. When the two axes are parallel or skew, the origin is located at the intersection of z_i with the common perpendicular of z_{i-1} and z_i. The x_i-axis is taken along this common perpendicular, pointing from z_{i-1} toward z_i; if the axes intersect, x_i is chosen along any direction perpendicular to both axes. The y_i-axis is determined by the right-hand rule.

This definition of coordinate frames ensures consistent parameter representation between adjacent links, thereby making the kinematic derivation process clear and reproducible.

2.3.1 *Derivation of Homogeneous Transformations Between Links*

In kinematic analysis, it is necessary to establish the coordinate transformation between two adjacent frames $\{i-1\}$ and $\{i\}$. According to the D-H convention, this transformation can be decomposed into four basic steps:

(1) Rotate about the z_{i-1}-axis by θ_i:

The frame $\{i-1\}$ is rotated around z_{i-1} by the joint angle θ_i, denoted as $R(z_{i-1}, \theta_i)$.

The corresponding homogeneous rotation matrix is given in Eq. (1):

$$R(z_{i-1},\theta_i) = \begin{bmatrix} \cos\theta_i & -\sin\theta_i & 0 & 0 \\ \sin\theta_i & \cos\theta_i & 0 & 0 \\ 0 & 0 & 1 & 0 \\ 0 & 0 & 0 & 1 \end{bmatrix} \tag{1}$$

(2) Translate along the z_{i-1}-axis by d_i:

The frame $\{i-1\}$ is translated along z_{i-1} by the link offset d_i, denoted as $T(z_{i-1}, d_i)$.

The homogeneous translation matrix is shown in Eq. (2):

$$T(z_{i-1},d_i) = \begin{bmatrix} 1 & 0 & 0 & 0 \\ 0 & 1 & 0 & 0 \\ 0 & 0 & 1 & d_i \\ 0 & 0 & 0 & 1 \end{bmatrix} \tag{2}$$

(3) Translate along the x_{i-1}-axis by a_i:

The frame $\{i-1\}$ is translated along x_{i-1} by the link length a_i, denoted as $T(x_{i-1}, a_i)$.

The homogeneous translation matrix is given in Eq. (3):

$$T(x_{i-1},a_i) = \begin{bmatrix} 1 & 0 & 0 & a_i \\ 0 & 1 & 0 & 0 \\ 0 & 0 & 1 & 0 \\ 0 & 0 & 0 & 1 \end{bmatrix} \tag{3}$$

(4) Rotate about the x_i-axis by α_i:

Finally, the frame is rotated about the x_i-axis by the link twist angle α_i, denoted as $R(x_i, \alpha_i)$. The corresponding homogeneous rotation matrix is provided in Eq. (4).

$$R(x_i,\alpha_i) = \begin{bmatrix} 1 & 0 & 0 & 0 \\ 0 & \cos\alpha_i & -\sin\alpha_i & 0 \\ 0 & \sin\alpha_i & \cos\alpha_i & 0 \\ 0 & 0 & 0 & 1 \end{bmatrix} \tag{4}$$

Therefore, the homogeneous transformation matrix between two adjacent link frames can be written as:

$$^{i-1}T_i = R(z_{i-1},\theta_i)T(z_{i-1},d_i)T(x_{i-1},a_i)R(x_i,\alpha_i) \tag{5}$$

which can be arranged into the standard D-H form as:

$$^{i-1}T_i = \begin{bmatrix} \cos\theta_i & -\sin\theta_i\cos\alpha_i & \sin\theta_i\sin\alpha_i & a_i\cos\theta_i \\ \sin\theta_i & \cos\theta_i\cos\alpha_i & -\cos\theta_i\sin\alpha_i & a_i\sin\theta_i \\ 0 & \sin\alpha_i & \cos\alpha_i & d_i \\ 0 & 0 & 0 & 1 \end{bmatrix} \tag{6}$$

When a manipulator has n degrees of freedom, the pose transformation of the end-effector frame $\{n\}$ with respect to the base frame $\{0\}$ can be obtained by successive multiplication of the adjacent transformations:

$$^0T_n = {}^0T_1\,{}^1T_2\cdots{}^{n-1}T_n \tag{7}$$

This homogeneous transformation representation is applicable not only to planar manipulators but also to spatial multi-DOF mechanisms, providing the foundation for subsequent forward and inverse kinematic solutions.

3 Kinematic Analysis of the Robot

This chapter investigates a three-link planar manipulator and develops its analytical forward and inverse kinematic models. According to the mechanism topology, the link parameters and joint variables are identified. The D-H parameter method is then employed to assign coordinate frames and derive the homogeneous transformation matrices, from which a closed-form forward kinematics expression for the end-effector pose is obtained. In addition, an analytical inverse kinematics solution is presented by combining geometric decomposition and the law of cosines.

3.1 Robot Model and Parameter Definition

The three-link planar manipulator consists of three rigid links connected in series by three revolute joints. All joint rotation axes are perpendicular to the plane of motion; thus, the overall motion of the manipulator can be regarded as serial planar rotation within a single plane. The structure of the three-link planar manipulator is shown in Figure 2.

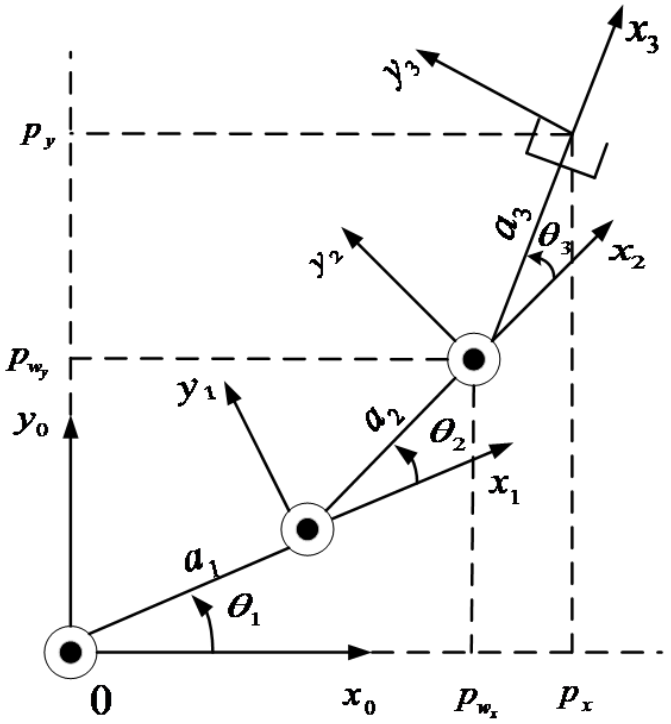

Figure 2. Structural diagram of the Three-Link Planar Manipulator.

As shown in Figure 2, the link lengths are denoted by a_1, a_2, and a_3, and the joint variables are θ_1, θ_2, and θ_3. A base coordinate frame $\{0\}$ is established at the robot base, and joint frames $\{1\}$, $\{2\}$, and $\{3\}$ are assigned sequentially along the kinematic chain, where frame $\{3\}$ is fixed to the end-effector. The end-effector position in the base frame is expressed as (p_x, p_y).

3.2 D-H Modeling and Homogeneous Transformation Matrices

To achieve a standardized representation of the serial manipulator kinematics, the D–H parameter method is adopted. Following the coordinate-frame assignment shown in Figure 2, the corresponding D–H parameter table is obtained, as listed in Table 1.

Table 1. D-H parameters of the Manipulator.

Link i	a_i	α_i	d_i	θ_i
1	a_1	0	0	θ_1
2	a_2	0	0	θ_2
3	a_3	0	0	θ_3

Since the manipulator is a planar 3R serial structure, the axes of adjacent joints are parallel and there is no link twist. Therefore, we set $\alpha_i = 0$ and $d_i = 0$. The homogeneous transformation matrix between adjacent link frames can thus be written as:

$$ {}^{i-1}_{i}T = \begin{bmatrix} \cos\theta_i & -\sin\theta_i & 0 & a_i\cos\theta_i \\ \sin\theta_i & \cos\theta_i & 0 & a_i\sin\theta_i \\ 0 & 0 & 1 & 0 \\ 0 & 0 & 0 & 1 \end{bmatrix} \tag{8} $$

According to Eq. (8), the transformation matrix of each link can be obtained as follows:

$$ {}^{0}_{1}T = \begin{bmatrix} \cos\theta_1 & -\sin\theta_1 & 0 & a_1\cos\theta_1 \\ \sin\theta_1 & \cos\theta_1 & 0 & a_1\sin\theta_1 \\ 0 & 0 & 1 & 0 \\ 0 & 0 & 0 & 1 \end{bmatrix} \tag{9} $$

$$ {}^{1}_{2}T = \begin{bmatrix} \cos\theta_2 & -\sin\theta_2 & 0 & a_2\cos\theta_2 \\ \sin\theta_2 & \cos\theta_2 & 0 & a_2\sin\theta_2 \\ 0 & 0 & 1 & 0 \\ 0 & 0 & 0 & 1 \end{bmatrix} \tag{10} $$

$$ {}^{2}_{3}T = \begin{bmatrix} \cos\theta_3 & -\sin\theta_3 & 0 & a_3\cos\theta_3 \\ \sin\theta_3 & \cos\theta_3 & 0 & a_3\sin\theta_3 \\ 0 & 0 & 1 & 0 \\ 0 & 0 & 0 & 1 \end{bmatrix} \tag{11} $$

3.3 Forward Kinematics Solution

The objective of forward kinematics is to determine the pose of the end-effector for given joint angles. According to the homogeneous transformation rule, the pose of the end-effector frame $\{3\}$ with respect

to the base frame $\{0\}$ is obtained by multiplying the adjacent transformations:

$$ {}^{0}T_{3} = {}^{0}T_{1}\,{}^{1}T_{2}\,{}^{2}T_{3} = \begin{bmatrix} r_{11} & r_{12} & r_{13} & p_x \\ r_{21} & r_{22} & r_{23} & p_y \\ r_{31} & r_{32} & r_{33} & p_z \\ 0 & 0 & 0 & 1 \end{bmatrix} \tag{12} $$

The explicit expressions of the parameters in Eq. (12) are given by:

$$ \begin{cases} r_{11} = \cos(\theta_1+\theta_2+\theta_3) \\ r_{12} = -\sin(\theta_1+\theta_2+\theta_3) \\ r_{13} = 0 \\ r_{21} = \sin(\theta_1+\theta_2+\theta_3) \\ r_{22} = \cos(\theta_1+\theta_2+\theta_3) \\ r_{23} = 0 \\ r_{31} = 0 \\ r_{32} = 0 \\ r_{33} = 1 \end{cases} \tag{13} $$

$$ \begin{aligned} p_x &= a_1\cos\theta_1 + a_2\cos(\theta_1+\theta_2) + a_3\cos(\theta_1+\theta_2+\theta_3) \\ p_y &= a_1\sin\theta_1 + a_2\sin(\theta_1+\theta_2) + a_3\sin(\theta_1+\theta_2+\theta_3) \\ p_z &= 0 \end{aligned} \tag{14} $$

The end-effector orientation angle φ satisfies

$$ \varphi = \theta_1+\theta_2+\theta_3 \tag{15} $$

These results indicate that the end-effector pose of the three-link planar manipulator is determined by the cumulative effect of the joint angles, and the expressions exhibit clear geometric interpretability. Specifically, the first term represents the projection contribution of the first link, while the second and third terms correspond to the projected superposition of the subsequent links under composite joint rotations.

3.4 Inverse Kinematics Solution

Given the desired end-effector pose matrix T, the process of solving for the corresponding joint variables θ_n is referred to as inverse kinematics. For a three-link planar manipulator, the forward kinematics couples position and orientation in a nonlinear manner. If the three joint angles are solved directly, the computation becomes cumbersome and the geometric meaning is not explicit. To simplify the derivation and improve interpretability, this paper introduces the "wrist point" concept [**?**]. Specifically, the inverse kinematics of the 3R manipulator is converted into a combined solution of "locating the wrist point with the first two links (2R) + compensating the end-effector orientation with the third joint."

Let the wrist-point coordinates be p_{W_x}, p_{W_y}. According to the forward kinematics in Eq. (13), the wrist point can be obtained by retracting the third link along the end-effector direction, yielding:

$$ \begin{aligned} p_{W_x} &= p_x - a_3\cos\varphi = a_1\cos\theta_1 + a_2\cos(\theta_1+\theta_2) \\ p_{W_y} &= p_y - a_3\sin\varphi = a_1\sin\theta_1 + a_2\sin(\theta_1+\theta_2) \end{aligned} \tag{16} $$

Thus, the inverse kinematics problem is reduced to determining the wrist-point position of a planar two-link mechanism. The distance from the wrist point to the base origin satisfies:

$$ p_{W_x}^2 + p_{W_y}^2 = a_1^2 + a_2^2 + 2a_1a_2\cos\theta_2 \tag{17} $$

Rearranging Eq. (16) gives the cosine expression for the second joint angle as:

$$ \cos\theta_2 = \frac{p_{W_x}^2 + p_{W_y}^2 - a_1^2 - a_2^2}{2a_1a_2} \tag{18} $$

From Eq. (17), the necessary condition for the existence of inverse solutions is $-1 \le \cos\theta_2 \le 1$, otherwise the target point lies outside the reachable workspace of the manipulator. Further, let $\sin\theta_2 = \pm\sqrt{1-\cos^2\theta_2}$, where the "+" sign corresponds to the elbow-down configuration and the "-" sign corresponds to the elbow-up configuration, reflecting the multiple-solution nature of inverse kinematics. Hence, the second joint angle can be obtained as:

$$ \theta_2 = \operatorname{atan2}(\sin\theta_2, \cos\theta_2) \tag{19} $$

After θ_2 is determined, substituting it into Eq. (15) yields the equations for θ_1:

$$ \begin{aligned} \sin\theta_1 &= \frac{(a_1+a_2\cos\theta_2)p_{W_y} - a_2\sin\theta_2 p_{W_x}}{p_{W_x}^2 + p_{W_y}^2} \\ \cos\theta_1 &= \frac{(a_1+a_2\cos\theta_2)p_{W_x} + a_2\sin\theta_2 p_{W_y}}{p_{W_x}^2 + p_{W_y}^2} \end{aligned} \tag{20} $$

Therefore, the first joint angle is computed by:

$$ \theta_1 = \operatorname{atan2}(\sin\theta_1, \cos\theta_1) \tag{21} $$

Finally, using the end-effector orientation constraint in Eq. (14), the third joint angle is directly obtained as:

$$ \theta_3 = \varphi - \theta_1 - \theta_2 \tag{22} $$

At this point, the closed-form inverse kinematics of the 3-DOF three-link planar manipulator is fully derived. Since two analytical branches (elbow-up and elbow-down) exist, an explicit branch-selection strategy is required in practice to avoid discontinuous joint commands. First, candidate solutions that violate joint limits are discarded; then the remaining feasible branch is selected by minimizing the joint variation with respect to the previous time step. This continuity-preserving rule suppresses branch switching and yields smooth joint trajectories suitable for real-time control. Application constraints such as obstacle avoidance can be incorporated in the feasibility filtering stage.

3.5 Verification of the Kinematic Model

To verify the correctness and applicability of the analytical forward and inverse kinematic models of the three-link planar manipulator, a three-link planar manipulator simulation model is established using the MATLAB Robotics Toolbox, and the toolbox outputs are compared with the analytical results. In the simulation, the link lengths are set to $a = [1, 1, 1]$. The corresponding manipulator model is shown in Figure 3.

3.5.1 Forward Kinematics Verification

The purpose of forward kinematics verification is to confirm that, for a given joint variable vector $q = [\theta_1, \theta_2, \theta_3]^T$, the end-effector pose matrix obtained from the analytical derivation matches the numerical result computed by the Robotics Toolbox. For this purpose, a representative set of joint angles is selected as

$$q = \left[\frac{\pi}{6}, \frac{\pi}{2}, \frac{\pi}{4}\right]^T,$$

which is substituted into both the analytical forward kinematics model and the toolbox model to solve the end-effector pose.

The pose matrix obtained from the analytical forward kinematics is:

$${}^0T_3 = \begin{bmatrix} -0.9659 & -0.2588 & 0 & -0.5999 \\ 0.2588 & -0.9659 & 0 & 1.6248 \\ 0 & 0 & 1 & 0 \\ 0 & 0 & 0 & 1 \end{bmatrix} \tag{23}$$

The numerical result computed by the Robotics Toolbox is shown in Figure 4.

The comparison indicates that the two results are identical in both the rotation submatrix and the translation vector, demonstrating that the established D-H parameterized model is correct and that the forward kinematics derivation is error-free.

3.5.2 Inverse Kinematics Verification

The objective of the inverse kinematics verification is to confirm that, for a given target end-effector pose, the analytical inverse solution can recover the original joint-angle input, thereby ensuring that the inverse kinematics procedure is correct and feasible. Specifically, the end-effector pose matrix $\mathbf{T}$ obtained in Section 4.1.1 is used as the inverse-kinematics input and substituted into the analytical inverse kinematics model to compute the joint angles, which are then compared with the original joint variables. The computed results are shown in Figure 5.

As illustrated in Figure 5, the joint angles obtained from the analytical inverse kinematics coincide with the given joint angles, thus realizing a closed-loop validation of "forward solution - inverse solution - recovery. " This demonstrates that the inverse kinematics derivation is correct and that the solution process is stable and reliable.

Through the above simulation-based verification, the numerical results from the MATLAB Robotics Toolbox remain highly consistent with the analytical derivations in both forward and inverse directions. Therefore, the three-link planar manipulator kinematic model established in this study is proven to be accurate and dependable, providing a solid theoretical basis for subsequent three-dimensional simulation, dynamic analysis, and control algorithm design.

3.6 Kinematic Simulation of the Manipulator

To further validate the rationality of the kinematic model of the three-link planar manipulator from a three-dimensional perspective, and to visually examine the motion responses of each joint and the end-effector under prescribed driving laws, this section conducts a co-simulation study using SolidWorks 3D modeling and ADAMS kinematic/dynamic simulation. First, the geometric model of the manipulator is built in SolidWorks and assigned material and mass properties. The model is then imported into ADAMS, where revolute joint constraints and driving functions are defined to analyze the motion characteristics of the manipulator under periodic excitation. The three-dimensional model of the manipulator is shown in Figure 6.

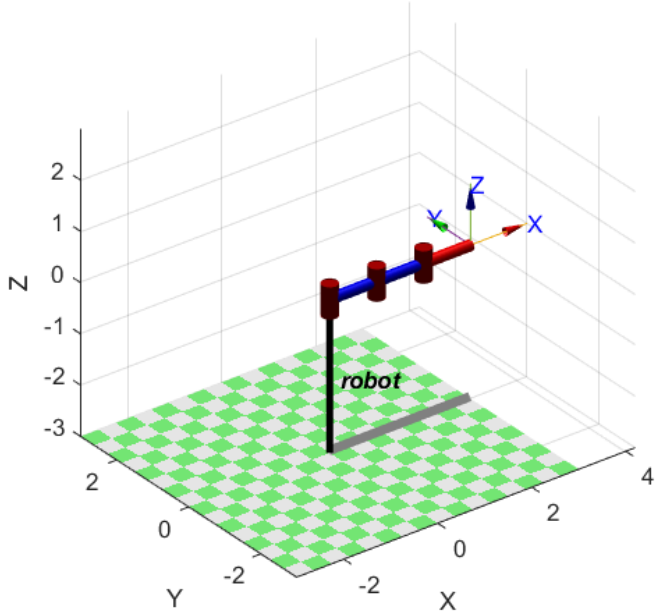

Figure 3. MATLAB model of the Manipulator.

```
T =
   -0.9659   -0.2588         0   -0.5999
    0.2588   -0.9659         0    1.625
         0         0         1         0
         0         0         0         1
```

Figure 4. Results computed by the Robotics Toolbox.

```
Q =

   30.0000   90.0000   45.0000
```

Figure 5. Joint-angle calculation results.

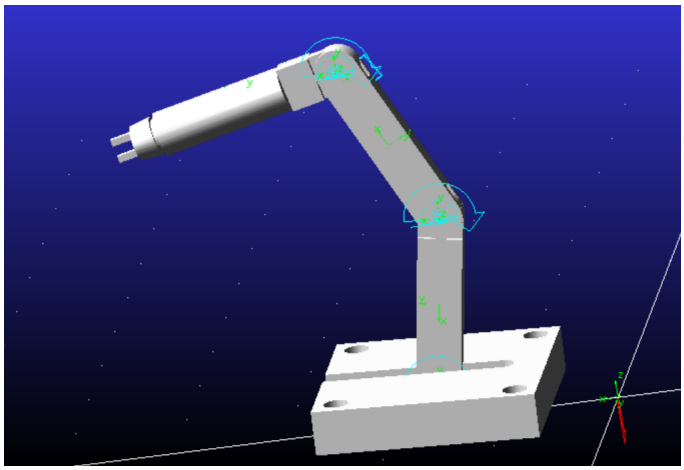

Figure 6. Three-dimensional model of the manipulator.

3.6.1 Driving Function Setup and Simulation Conditions

To achieve smooth periodic oscillation of the joints and to emulate a typical trajectory-planning effect, sinusoidal angular-displacement inputs are applied to all three revolute joints. The driving functions are specified as follows:

$$\begin{aligned} \theta_1 &= -15^\circ \sin(180^\circ t - 90^\circ) - 15^\circ \\ \theta_2 &= 15^\circ \sin(145^\circ t - 90^\circ) + 15^\circ \\ \theta_3 &= 45^\circ \sin(180^\circ t - 90^\circ) + 45^\circ \end{aligned} \tag{24}$$

Here, the sinusoidal terms ensure continuous and smooth joint motion, while the constant offsets constrain each joint to oscillate within a reasonable working range. The amplitudes of the three joints are set to 15°, 15°, and 45°, respectively, which follows the common planning strategy of "small-amplitude motion near the base and larger-amplitude swing toward the distal end." Moreover, the angular frequency of Joint 2 is intentionally set different from those of Joints 1 and 3, introducing a non-commensurate frequency coupling. This gives the end-effector trajectory a composite periodic characteristic, which facilitates evaluating the model's capability to represent coordinated multi-joint motion.

3.6.2 *Analysis of Joint Angular-Displacement Responses*

Under the above driving constraints, the time histories of the three joint angular displacements are shown in Figures 7, 8 and 9.

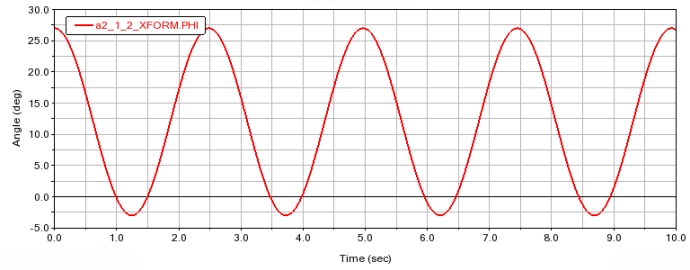

Figure 7. Angular Displacement of Joint 1.

As can be observed from Figure 7, the angular displacement of Joint 1 exhibits a standard sinusoidal variation, oscillating symmetrically about the offset angle of -15°. The waveform is smooth and continuous without abrupt changes, indicating that the revolute-joint constraint is stable and that the driving input has been correctly applied.

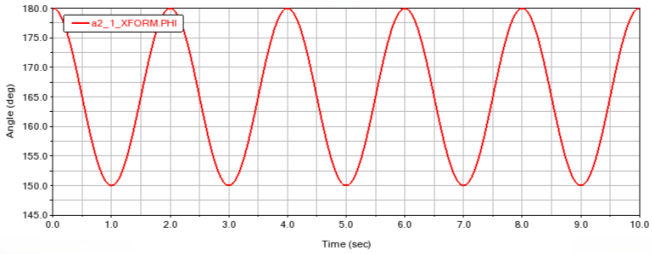

Figure 8. Angular Displacement of Joint 2.

From Figure 8, Joint 2 also shows a periodic sinusoidal response. However, due to its different driving frequency, its phase evolution is not synchronized with Joints 1 and 3, resulting in a progressive phase shift. This reflects the independent modulation role of the middle joint in generating a composite end-effector trajectory.

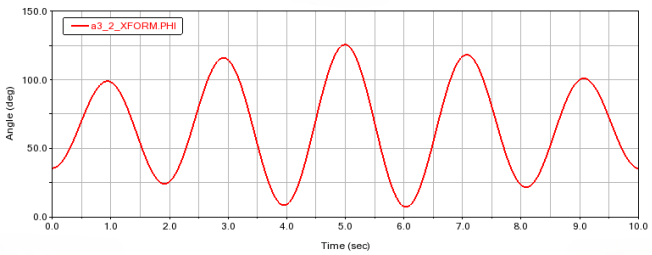

Figure 9. Angular Displacement of Joint 3.

As shown in Figure 9, Joint 3 exhibits the largest oscillation amplitude and the most pronounced angular variation, indicating that it mainly serves to adjust the end-effector orientation and local position.

Overall, the joint displacements strictly follow the prescribed driving laws without mutual coupling or interference, demonstrating that the manipulator configuration and constraint settings are correct.

3.6.3 *Simulation of Joint Angular Velocity and Angular Acceleration*

By taking the first- and second-order derivatives of the angular displacements, the joint angular-velocity and angular-acceleration responses can be obtained, as shown in Figures 10, 11 and 12. In these figures, the solid lines represent angular velocity, and the dashed lines represent angular acceleration.

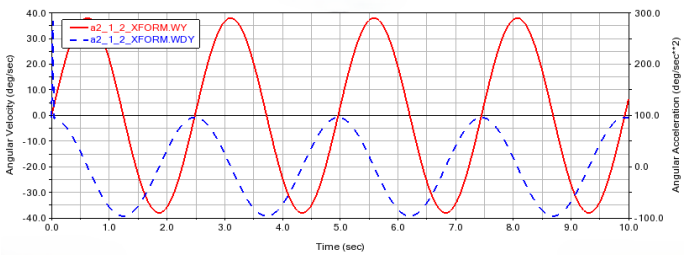

Figure 10. Angular Velocity and Angular Acceleration of Joint 1.

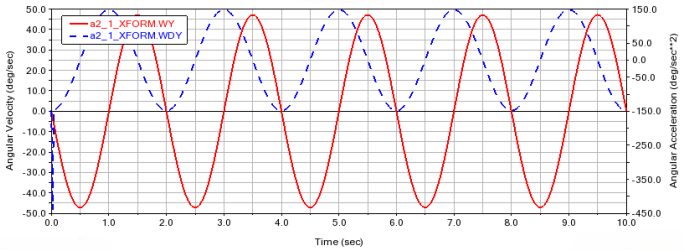

Figure 11. Angular Velocity and Angular Acceleration of Joint 2.

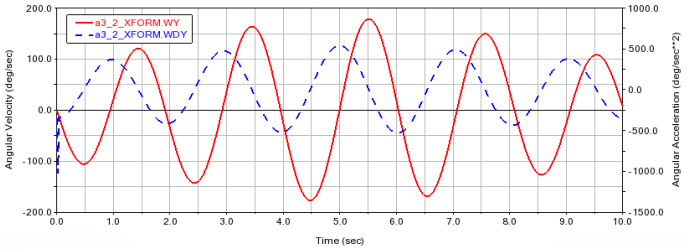

Figure 12. Angular Velocity and Angular Acceleration of Joint 3.

As shown in Figures 10, 11 and 12, under sinusoidal angular-displacement excitation, the angular-velocity curves correspond to the first derivative of the

displacement and thus exhibit cosine-like periodic variations. Specifically, the angular velocity reaches its maximum near the zero-crossings of the displacement and decreases to zero at the displacement peaks and troughs. The angular-acceleration curves are the second derivative of the displacement; they have the same frequency as the displacement but an opposite phase. The maximum negative acceleration occurs at the displacement peaks, while the maximum positive acceleration appears at the troughs. This behavior reflects the periodic switching of each joint through "acceleration-deceleration-reverse acceleration" during the oscillatory motion.

3.6.4 End-Effector Displacement Simulation

A measurement point is defined at the end-effector to obtain its displacement responses in the $x-$, $y-$, and $z-$directions, as shown in Figures 13, 14 and 15.

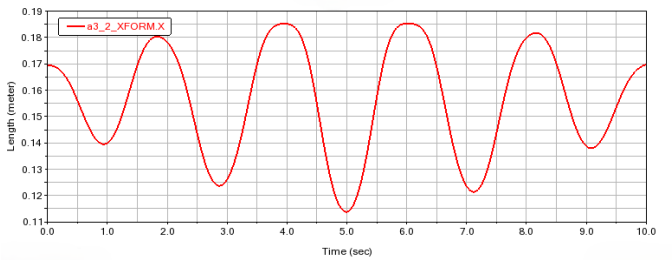

Figure 13. Displacement Along the x-Axis.

As shown in Figure 13, the displacement exhibits a clear periodic fluctuation. Its dominant frequency is jointly determined by the synchronous driving of Joints 1 and 3, reflecting the horizontal sweeping range of the end-effector within the planar workspace.

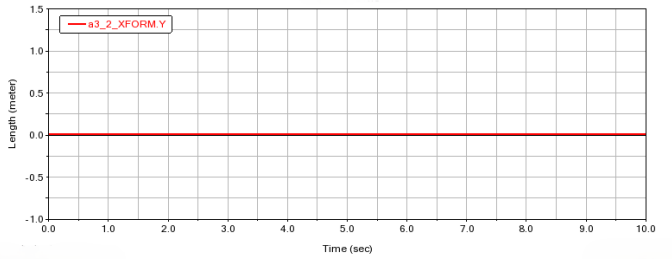

Figure 14. Displacement Along the y-Axis.

As shown in Figure 14, the displacement remains essentially constant, indicating that under the current coordinate definition and joint-constraint configuration, the manipulator moves primarily in the $x-z$ plane. This observation is consistent with the structural characteristics of a three-link planar mechanism.

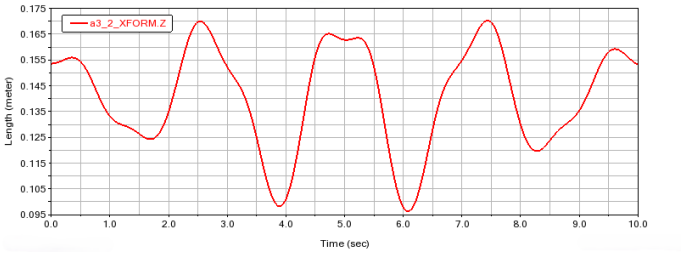

Figure 15. Displacement Along the z-Axis.

As shown in Figure 15, the displacement also varies periodically. Compared with the z-direction, however, it shows a more pronounced composite modulation pattern. This is caused by the superposition of Joint 2's excitation at a different frequency with the motions of the other joints, resulting in an amplitude-modulated variation of the end-effector in the vertical direction that is not strictly single-periodic.

The SolidWorks–ADAMS three-dimensional co-simulation further confirms the correctness of the kinematic model for the 3-DOF three-link planar manipulator. The results demonstrate that (i) the joint angular displacements strictly follow the prescribed driving functions and remain stable; (ii) the angular-velocity and angular-acceleration responses are consistent with the derivative relationships of sinusoidal displacement inputs, with reasonable peak distributions; (iii) the end-effector displacements exhibit continuous periodic variations, while the y-direction displacement is approximately constant, verifying the planar-mechanism motion characteristics; and (iv) no abnormal oscillations or unreachable poses occur during motion, indicating that the model and constraint settings are properly configured.

4 Conclusions

This paper investigates a three-degree-of-freedom (3-DOF) three-link planar serial manipulator, focusing on its kinematic modeling, closed-form solutions, and simulation consistency. First, based on the mechanism topology and geometric relationships, the Denavit-Hartenberg (D-H) parameterization method is employed to assign link coordinate frames and derive the homogeneous transformation matrices. A closed-form forward kinematics expression relating the end-effector pose to the joint variables is obtained, which clearly reveals the planar serial motion principle: the end-effector position results from the superposition of the projected link vectors, while its orientation is determined by the cumulative sum of the three joint angles. Second, using

wrist-point retraction and geometric decomposition, the inverse kinematics problem is reduced to a two-dimensional two-link positioning task combined with an end-effector orientation constraint. This yields analytical closed-form solutions for the joint angles, and the symmetric multiple-solution configurations (elbow-up and elbow-down) as well as their reachability conditions are analyzed. Subsequently, a numerical model is established in the MATLAB Robotics Toolbox and a closed-loop "forward-inverse-recovery" validation is performed. The results show excellent agreement between the analytical solutions and the numerical outputs. Furthermore, SolidWorks–ADAMS three-dimensional co-simulation under periodic sinusoidal driving confirms that the joint motions and end-effector trajectories are smooth, continuous, and consistent with the theoretical derivations. In summary, this study constructs and validates a complete analytical framework for the forward and inverse kinematics of a three-link planar manipulator, providing a reliable foundation for future work on dynamics modeling, trajectory planning, and control algorithm development.

Data Availability Statement

Data will be made available on request.

Funding

This work was supported without any funding.

Conflicts of Interest

The author declares no conflicts of interest.

AI Use Statement

The author declares that no generative AI was used in the preparation of this manuscript.

Ethical Approval and Consent to Participate

Not applicable.

References

[1] Craig, J. J. (2009). *Introduction to robotics: mechanics and control, 3/E*. Pearson Education India.

[2] Bartoš, M., Bulej, V., Bohušík, M., Stanček, J., Ivanov, V., & Macek, P. (2021). An overview of robot applications in automotive industry. *Transportation Research Procedia, 55*, 837–844. [CrossRef]

[3] Siciliano, B., Khatib, O., & Kröger, T. (Eds.). (2008). *Springer handbook of robotics* (Vol. 200, p. 1). Berlin: springer. [CrossRef]

[4] Corke, P. I., Jachimczyk, W., & Pillat, R. (2011). *Robotics, vision and control: fundamental algorithms in MATLAB* (Vol. 73, p. 2). Berlin: Springer. [CrossRef]

[5] Spong, M. W., Hutchinson, S., & Vidyasagar, M. (2020). Robot modeling and control. *John Wiley & amp*. [CrossRef]

[6] Lynch, K. M., & Park, F. C. (2017). *Modern Robotics: Mechanics, Planning, and Control*. Cambridge University Press. [CrossRef]

[7] Angeles, J. (Ed.). (2003). *Fundamentals of robotic mechanical systems: theory, methods, and algorithms*. New York, NY: Springer New York. [CrossRef]

[8] Khalil, W., & Dombre, E. (2002). *Modeling, Identification and Control of Robots*. Butterworth-Heinemann.

[9] Kucuk, S., & Bingul, Z. (2006). Robot Kinematics: Forward and Inverse Kinematics. In *Industrial Robotics: Theory, Modelling and Control*. IntechOpen. [CrossRef]

[10] Urrea, C., & Kern, J. (2025). Recent Advances and Challenges in Industrial Robotics: A Systematic Review of Technological Trends and Emerging Applications. *Processes, 13*(3), 832. [CrossRef]

[11] Paul, R. P. (1981). *Robot Manipulators: Mathematics, Programming, and Control*. MIT Press.

[12] Waseem, S., Adnan, M., Iqbal, M. S., Amin, A. A., Shah, A., & Tariq, M. (2025). From classical to intelligent control: Evolving trends in robotic manipulator technology. *Computers and Electrical Engineering, 127*, 110559. [CrossRef]

[13] Pieper, D. L. (1969). *The kinematics of manipulators under computer control*. Stanford University.

[14] Featherstone, R. (2008). *Rigid Body Dynamics Algorithms*. Springer. [CrossRef]

[15] Tinoco, V., Silva, M. F., Santos, F. N., Morais, R., Magalhães, S. A., & Oliveira, P. M. (2025). A review of advanced controller methodologies for robotic manipulators. *International Journal of Dynamics and Control, 13*(1), 36. [CrossRef]

[16] Tsai, L. W. (1999). Robot analysis: the mechanics of serial and parallel manipulators. John Wiley & Sons.

[17] Selig, J. M. (2005). *Geometric fundamentals of robotics*. New York, NY: Springer New York. [CrossRef]

[18] Zhang, W., Chen, R., Chen, H., You, Z., & Zhao, Y. (2025). Research on a New Pre-defined Time Sliding Mode Control Method for Nonlinear Systems. *IAENG International Journal of Applied Mathematics, 55*(8), 2482–2488.

[19] Manocha, D., & Canny, J. F. (1994). Efficient inverse kinematics for general 6R manipulators. *IEEE Transactions on Robotics and Automation, 10*(5), 648–657. [CrossRef]

[20] Jazar, R. N. (2010). *Theory of Applied Robotics: Kinematics, Dynamics, and Control* (2nd ed.). Springer. [CrossRef]

[21] Merlet, J. P. (2006). *Parallel robots*. Dordrecht: Springer Netherlands. [CrossRef]

[22] Sciavicco, L., & Siciliano, B. (2012). *Modelling and Control of Robot Manipulators* (2nd ed.). Springer. [CrossRef]

[23] Murray, R. M., Li, Z., & Sastry, S. S. (1994). *A Mathematical Introduction to Robotic Manipulation*. CRC Press. [CrossRef]

[24] Siciliano, B., & Khatib, O. (2016). Robotics and the handbook. In *Springer Handbook of Robotics* (pp. 1-6). Cham: Springer International Publishing. [CrossRef]

[25] Mason, M. T. (2001). *Mechanics of Robotic Manipulation*. MIT Press. [CrossRef]

[26] Ghosal, A. (2006). *Robotics: Fundamental Concepts and Analysis*. Oxford University Press.

[27] Sharkawy, A. N., & Khairullah, S. S. (2023). Forward and Inverse Kinematics Solution of A 3-DOF Articulated Robotic Manipulator Using Artificial Neural Network. *International Journal of Robotics & Control Systems, 3*(2), 340–357. [CrossRef]

[28] Zaplana, I., Hadfield, H., & Lasenby, J. (2022). Closed-form solutions for the inverse kinematics of serial robots using conformal geometric algebra. *Mechanism and Machine Theory, 173*, 104835. [CrossRef]

[29] Denavit, J., & Hartenberg, R. S. (1955). A kinematic notation for lower-pair mechanisms based on matrices. *Journal of Applied Mechanics, 22*(2), 215–221. [CrossRef]

[30] Kucuk, S., & Bingul, Z. (2014). Inverse kinematics solutions for industrial robot manipulators with offset wrists. *Applied Mathematical Modelling, 38*(7–8), 1983–1999. [CrossRef]

Nuoyu Jiang received the B.Eng. degree in Intelligent Equipment and Systems from Yancheng Institute of Technology, Yancheng, China, in 2024. He is currently pursuing the M.S. degree with Yancheng Institute of Technology, Yancheng, China. (Email: jiangnuoyu2025@126.com)